NANO LETTERS

Letter

pubs.acs.org/NanoLett

# Biomimetic Ant-Nest Electrode Structures for High Sulfur Ratio Lithium−Sulfur Batteries

Guo Ai,[†,‡] Yiling Dai,[†] Wenfeng Mao,[†,§] Hui Zhao,[†] Yanbao Fu,[†] Xiangyun Song,[†] Yunfei En,[‡] Vincent S. Battaglia,[†] Venkat Srinivasan,[†] and Gao Liu*[,†]

[†]Energy Storage and Distributed Resources Division, Energy Technologies Area, Lawrence Berkeley National Laboratory, Berkeley, California 94720, United States

[‡]Science and Technology on Reliability Physics and Application of Electronic Component Laboratory, No. 5 Electronic Research Institute of the Ministry of Industry and Information Technology, Guangzhou 510610, China

[§]Guangzhou Automobile Group Co., Ltd., Guangzhou 511434, China

*S* *Supporting Information*

**ABSTRACT:** The lithium−sulfur (Li−S) rechargeable battery has the benefit of high gravimetric energy density and low cost. Significant research currently focuses on increasing the sulfur loading and sulfur/inactive-materials ratio, to improve life and capacity. Inspired by nature's ant-nest structure, this research results in a novel Li−S electrode that is designed to meet both goals. With only three simple manufacturing-friendly steps, which include slurry ball-milling, doctor-blade-based laminate casting, and the use of the sacrificial method with water to dissolve away table salt, the ant-nest design has been successfully recreated in an Li−S electrode. The efficient capabilities of the ant-nest structure are adopted to facilitate fast ion transportation, sustain polysulfide dissolution, and assist efficient precipitation. High cycling stability in the Li−S batteries, for practical applications, has been achieved with up to 3 mg·cm$^{-2}$ sulfur loading. Li−S electrodes with up to a 85% sulfur ratio have also been achieved for the efficient design of this novel ant-nest structure.

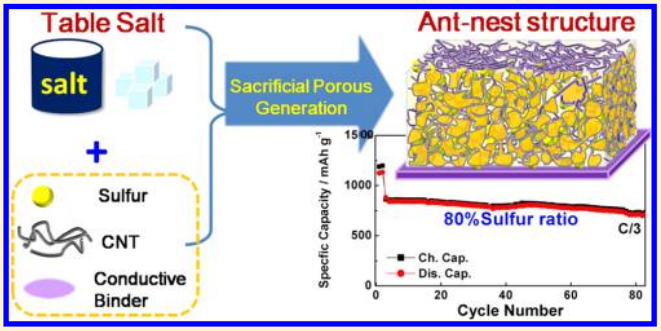


**KEYWORDS:** *Li−S battery, biomimetic, ant-nest structure, high sulfur ratio*

High energy density and low-cost rechargeable batteries are attracting great interest because of increasing manufacturing and consumer demand for portable devices, electric vehicles, and stationary energy storage systems that have longer charge times and overall battery lives.[1,2] The lithium−sulfur (Li−S) battery is one of the most promising candidates because of its high energy density (2600 W·h·kg$^{-1}$), environmental friendliness, and low cost due to the earth-abundant resource of elemental sulfur—which is also a byproduct from the petroleum industry.[3−6] However, the application of Li−S batteries has been hindered by several shortcomings, including poor cycling stability, low Coulombic efficiency, and practical low energy density at the cell level. These shortcomings primarily stem from the dissolution of polysulfide in the electrolyte as an intermediate species during both charge and discharge processes. The polysulfide could diffuse to and react with Li-metal electrode through the shuttle effect, resulting in active material loss and self-discharge.[7] A significant amount of research has addressed this issue, which includes studies and work to encapsulate the polysulfide with a well-designed structure,[8−12] attract polysulfide through functional groups with strong affinity,[13−18] and eliminate polysulfide dissolution with the design of an electrolyte,[19−21] modification of separator,[22,23] and so forth. Another issue that limits the performance of Li−S batteries is the poor electrical conductivity of the reaction products ($S_8$ in the charged state and $Li_2S/Li_2S_2$ in the discharged state), which is also an obstacle to the high utilization of the active material.[10] In most research works, conductive additives with a high weight ratio (40−50%) are incorporated into the electrode to solve this problem, and a complicated design of sulfur/carbon composites needs to be performed. Therefore, the active material (sulfur) content is low at the electrode level, and the practical energy density of the Li−S batteries suffers.[24] The next step in advancing Li−S technology is to design a high-efficiency Li−S electrode that can achieve high practical energy density, have good cycling stability, and minimize the composition of the inactive component (e.g., conductive additive, binder, current collector, etc.).

To achieve these application goals, additional high-loading Li−S battery research is critical as well as intriguing to the research community.[15,25,26] In the effort to maximize energy

**Received:** April 6, 2016
**Revised:** July 13, 2016
**Published:** August 8, 2016





DOI: 10.1021/acs.nanolett.6b01434
*Nano Lett.* 2016, 16, 5365−5372

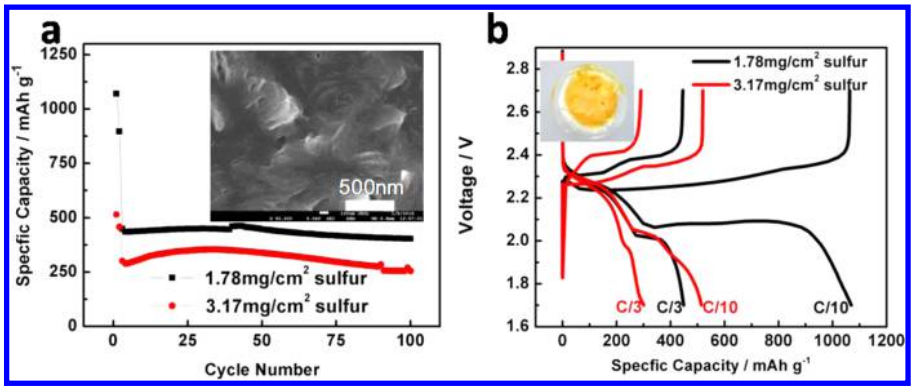


**Figure 1.** Cycling performance (a) and voltage profile (b) of the CNT-S cells with 1.78 mg·cm$^{-2}$ and 3.17 mg·cm$^{-2}$ sulfur loading. The SEM top morphology of the fully discharged CNT-S cell with 3.17 mg·cm$^{-2}$ sulfur loading is shown as an inset in panel a, and a photo image of the separator of the same cell is shown in panel b.

density in Li−S batteries, especially in high-power applications (e.g., high current output), the most predominant issue is blocking ion transportation channels.[24,27,28] In high-loading Li−S batteries, a significant amount of solid sulfur species ($S_8$ in the charged state and $Li_2S/Li_2S_2$ in the discharged state) will precipitate on the electrode/electrolyte interface during charge/discharge process.[29,30] Since they are highly insulating, the ion transportation channels in electrodes are likely to be blocked, which will result in poor sulfur utilization and severe shuttle effect. Another critical issue for high-loading Li−S batteries is that larger amounts of polysulfide dissolution lead to a much more severe shuttle effect. Therefore, the ability of the electrode to sustain the polysulfide well becomes a key issue. Also, mechanical issues arise as the electrode becomes thicker to increase area loading. Cracks and delamination in the electrode are common if the binder cannot carry the inner stress.[24] Therefore, to achieve a high-efficiency, high-loading Li−S battery, several properties of the Li−S design need to be addressed: first, enough interconnected and continuous open channels to facilitate fast Li-ion and polysulfide transportation; second, a large and highly conductive surface for polysulfide reaction and $S_8$ or $Li_2S/Li_2S_2$ precipitation; third, the capability of the electrode to retain polysulfide and mitigate their diffusion into the electrolyte.

To address these concerns, this research team integrated all of the design criteria and proposed a novel and highly efficient electrode structure for Li−S batteries in this work. The structure is inspired by nature's own superefficient ant nest. The structure of the ant-nest network is famous for the smart spacial design with abundant storage space and multi interconnected channels between storage sites, which allows for efficient and fast transportation of food.[31] The novel ant-nest electrode is fabricated using only three cost-effective industry-scale processing methods: ball-milling for slurry mixing, the doctor-blade method for laminate casting, and the feasible sacrificial method for porous creation. The multiwall carbon nanotube (CNT), known as the world's best conductive agent,[32] is selected for the conductive additive to enable ultrafast and long-distance electron transportation. Also, the large surface area of CNT can provide increased reaction interface for sulfur species precipitation. The functionalized conductive binder poly(9,9-dioctylfluorene-*co*-fluorenone-*co*-methylbenzoic ester) (PFM), designed in our group,[33] has been selected for the nest structure. The effect of conductive binder and the functionality in assisting the surface interaction has been well demonstrated with a detailed mechanism study.[17] Table salt (sodium chloride, NaCl), which costs little and is abundant and environmentally friendly, is selected as the sacrificial additive for the electrode design. After the laminate is casted, the NaCl microparticles are removed from composite electrode by simple water washing. A perfect ant-nest structure in the Li−S electrode is formed using this simple method; its key characteristics include multi-interconnected channels for ultrafast Li-ion transport, numerous micro/nano porous structures for sufficient polysulfide storage, and a large inner surface suitable for reaction interface. With this structural design, the ant-nest electrode shows good performance at sulfur loading up to 3 mg·cm$^{-2}$.

Moreover, due to the fact that the large weight ratio of inactive material, usually as high as 40−50%, will influence the energy density of Li−S batteries, current research suggests a critical need to create a Li−S battery with a higher sulfur ratio.[34] Research efforts pursuing this goal have had limited success.[26,35] In this team's work, using the ant-nest structure Li−S electrode, the sulfur composition can be pushed up to 85 wt %, with only 12 wt % CNT and 3 wt % binder at the electrode scale. This research demonstrates the potential of this ant-nest electrode via successful improving the loading and sulfur ratio of Li−S systems and is offered as advancement in Li−S battery technology.

In high-loading Li−S batteries, fast ion transport capability is the most crucial factor. But in most cases the transport is not sufficient due to the liable blocking of the transport channels and limited reaction surface, especially in the case of high rate requirement. This will lead to low cycling capacity and poor sulfur utilization.[24] In this work, the phenomena is demonstrated via two Li−S electrode systems using CNT and acetylene black (AB) as conductive additives, at different sulfur loadings, respectively. For Li−S cells with the CNT additive, named CNT-S, two different sulfur loadings of 1.78 mg·cm$^{-2}$ and 3.17 mg·cm$^{-2}$ are tested, shown in Figure 1a−b. Low actual capacity and sulfur utilization are observed in both cells, especially at C/3 and higher loading, and the area capacity for two cells is very similar, being below 1 mA·h·cm$^{-2}$, in Figure S1a. The main reason for this issue can be analyzed via the voltage profile, shown in Figure 1b. In the 1.78 mg·cm$^{-2}$ CNT-S cell, almost the same capacity is obtained from the upper voltage plateau both at C/10 and C/3, which corresponds to the long chain polysulfide dissolution (from $S_8$ to $Li_2S_4$); however, the capacity obtained from the lower voltage plateau shows a significant difference between C/10 and C/3. Only 200 mAh·g$^{-1}$ capacity can be obtained at C/3 in this region, which


DOI: 10.1021/acs.nanolett.6b01434
*Nano Lett.* 2016, 16, 5365−5372

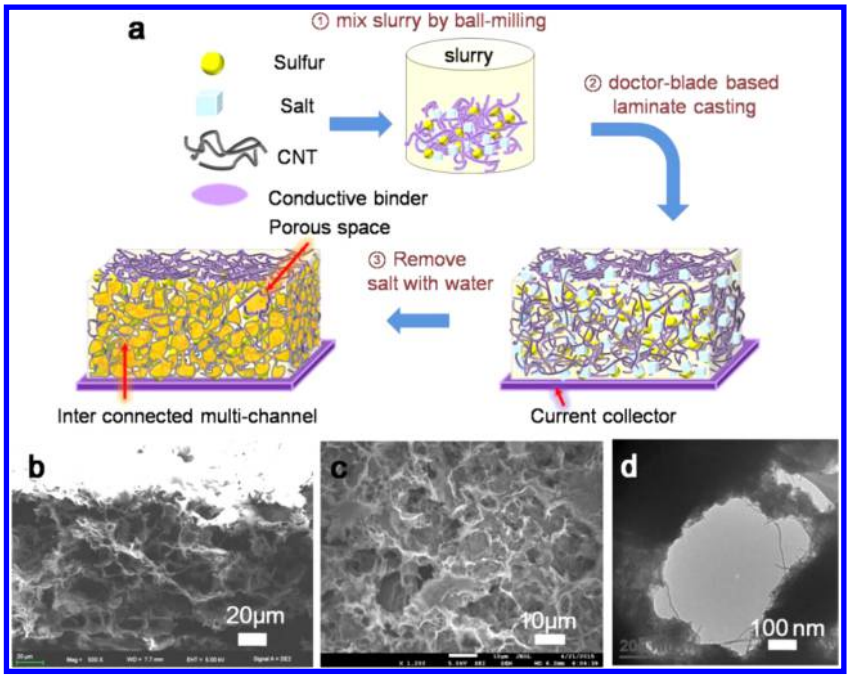


**Figure 2.** (a) Schematic illustration of the porous ant-nest structure Li−S electrode (CNT-nest-S) fabrication procedure. SEM cross-section (b) and top (c) morphology of CNT-nest-S. (d) The TEM morphology of the pore in the fully discharged CNT-nest-S.

is one-quarter of the 800 mAh·g$^{-1}$ obtained at C/10. This indicates that insufficient sulfur precipitation (from $Li_2S_4$ to $Li_2S$) exists in the second discharge plateau. This issue is more severe in Li−S electrodes with 3.17 mg·cm$^{-2}$ sulfur loading, in which the lower plateaus are severely reduced both at C/10 and C/3. This demonstrates that the electrode structure cannot support the simultaneous precipitation of a large quantity of polysulfide. This issue is also observed in different Li−S systems with AB as additive (see Figure S2).

The main cause of this insufficient $Li_2S$ precipitation is the blockage of the ion transport channel, which can be further elucidated via post-mortem analysis. A thick layer of $Li_2S$ precipitation is observed on the ∼3 mg·cm$^{-2}$ electrode after full discharge at C/3, shown in Figure 1a inset, but the internal pores are still empty, as shown in Figure S1. When current density is high, the sulfur species ($Li_2S_x$, $x$ = 1−2), which has a poor solubility and is highly insulating, is very likely to precipitate on the electrode surface next to the separator, blocking the small channels on the electrode surface. The electrode surface area is too small for efficient $Li_2S$ precipitation. The thick $Li_2S$ layer will lead to severe passivation of the electrode and early end of discharge, shown in Figure 1a. A large quantity of polysulfide will be blocked out and remain in the electrolyte, shown in Figure 1b inset, which leads to low actual capacity. Once the surface pores and channels are blocked, no more charge/discharge can take place even with a further increase of the sulfur loading. Therefore, ion transport channel blockage and insufficient reaction interface have been the major limiting factor in further attempts to achieve high loading for Li−S batteries, both of which can be overcome by using the ant-nest structure that is proposed and designed in this work.

In this work, the team integrates the above-discussed criteria into the design of a novel ant-nest electrode structure for Li−S batteries (named as CNT-nest-S), which is designed to imitate nature's own ant-nest structure, taking advantage of its abundant storage and highly efficient transport system. The team adopts the common, cheap, abundant, and environmental friendly table salt (NaCl) as the sacrificial additive, which can be easily ball-milled down to smaller than 10 $\mu$m in size. CNT, a well-known and highly efficient carrier transport agent with ultra high carrier mobility, is selected as a conductive additive for the Li−S batteries in this work. The CNTs are interconnected to enable long distance charge transport and are able to process large surface areas. A high efficient conductive binder, PFM, with functionality designed in our group is selected for the ant-nest Li−S system.[33] The assisting effect of conductivity and functionality in Li−S reaction mechanism has been systematically demonstrated in previous studies.[36] The salt is mixed directly with sulfur particles, binder, and CNT to form the slurry using the ball-milling method. After the laminate is casted via doctor-blade method, the NaCl microparticles are removed from the composite electrode with a simple water washing step, as shown in Figure 2a. A perfect ant-nest structure is formed with this simple method. The porous morphology of the ant-nest electrode structure can be demonstrated with the electrode cross-section and surface SEM morphology, as shown in Figure 2b−d. The microsize pores created by the templating NaCl crystals ensure numerous interconnected multi-ion channels, which both facilitate ion conduction and decrease the possibility of blockage by sulfur species precipitation. Both large and small pores exist in this ant-nest structure. The large microsize pores generated by the templating NaCl particles for polysulfide storage and sustention. The nanosize pores between nanotubes, created by solvent evaporation are connected to the micropores, enabling the fully utilization of CNT surfaces. Therefore, the template approach has significantly enlarged the reaction interface in the electrode.

The property of this structure meets all of the requirements for Li−S batteries: (1) the interconnected channels between storage sites enable fast ion and polysulfide transport and can prohibit channel blocking; (2) the nest structure features ample storage to efficiently sustain polysulfide as well as to



DOI: 10.1021/acs.nanolett.6b01434
Nano Lett. 2016, 16, 5365−5372

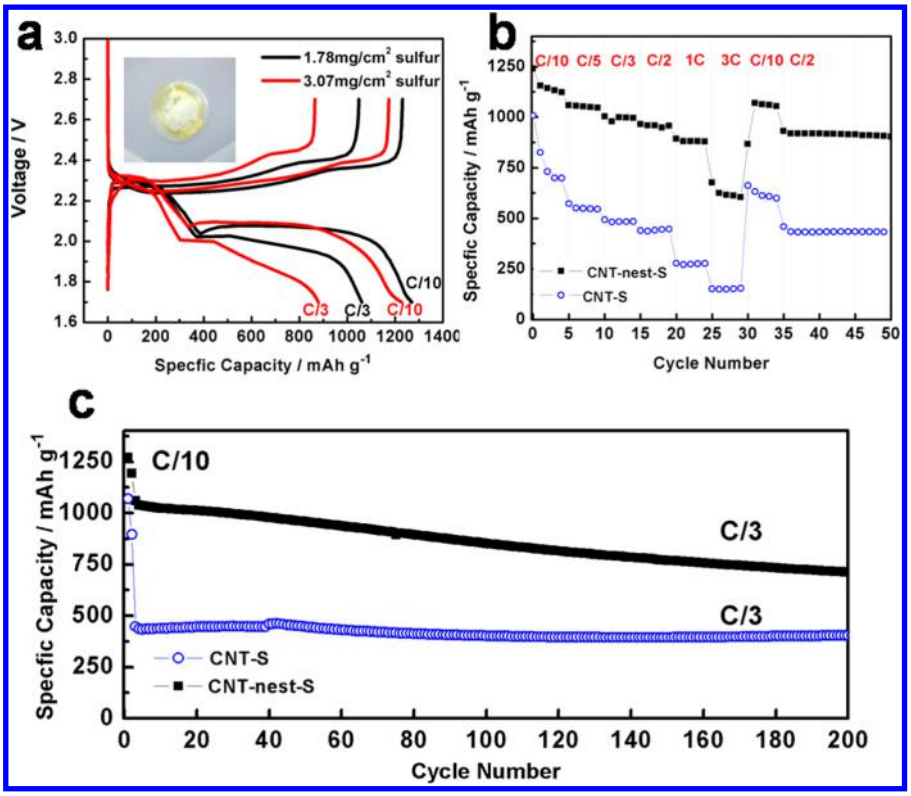


**Figure 3.** (a) Voltage profiles for the 1.78 mg·cm$^{-2}$ and 3.07 mg·cm$^{-2}$ CNT-nest-S cell at C/10 and C/3) and a photo image of the separator of the 3.07 mg·cm$^{-2}$ cell is shown in panel a, disassembled after two C/10 cycles and discharge at C/3. The comparison of rate performance (b) and cycling performance (c) between CNT-S and CNT-nest-S cell, with a sulfur loading of 1.78 mg·cm$^{-2}$.

accommodate sulfur volume change; (3) the maximized inner surface via the nest structure and the CNT facilitates efficient surface reaction for the transition among different sulfur species; (4) the functionalized conductive binder can help to further sustain the polysulfide inside storage pores with strong affinity between the functional binder and the polysulfide; (5) the conductive binder assists the interconnecting CNT framework in providing super conductivity and a long-distance charge transport pathway for the Li−S electrode; (6) the strong mechanical properties of CNT and the binder enable the structure the mechanical strength to sustain the volume change during phase transformation of sulfur species. The ant-nest structure method is cost-effective and facile and allows for electrode-level fabrication, using only table salt and water as processing ingredients.

The superior properties of the ant-nest structure can be demonstrated by examining its electrochemical performance, shown in Figure 3a−c. The two-plateau voltage profiles of CNT-nest-S cells of two loadings are similar both at C/10 and C/3, shown in Figure 3a, indicating the CNT-nest-S structure enables good ion transporting, as well as highly efficient sulfur dissolution (from $S_8$ to $Li_2S_4$) and precipitation (from $Li_2S_4$ to $Li_2S$), without the channel blocking issue, even at 3.07 mg·cm$^{-2}$ loading. Therefore, high sulfur utilization is achieved even at a high rate discharge.

The comparison between the cells with (CNT-nest-S) and without (CNT-S) the nest structure further demonstrate the benefits of the ant-nest structure design. The CNT-nest-S electrode possesses superior cycling performance and rate performance over CNT-S, shown in Figure 1 and Figure 3. With the same charge and discharge rates, the specific capacity for CNT-nest-S structure from C/10 to 1C is quite similar, and a capacity of 615 mA·h·g$^{-1}$ can still be obtained at 3C. In contrast, less than half of the capacity is obtained at levels higher than C/5 in a regular CNT-S cell; less than 200 mA·h·g$^{-1}$ can be obtained at 3C. As a further indication of the properties of CNT-nest-S structure, long-term cycling performance at C/3 is plotted in Figure 3c. The stable cycling specific capacity of 1060 mA·h·g$^{-1}$ is achieved for the CNT-nest-S cell, but only 445 mA·h·g$^{-1}$ is achieved for CNT-S. These data gives strong evidence to the capabilities and potential of the CNT-nest-S structure in facilitating Li−S batteries and achieving superior rate and cycling performance.

The high performance of the CNT-nest-S Li−S cells stems from the unique property of the nest structure. The working mechanism of the nest structure is demonstrated in the diagram in Figure 4a−c and the electrode structures via post-mortem analysis in Figure 4d−f. Several key mechanisms are of interest. First, the interconnected channels for ion transport are highly efficient in assisting ultrafast reaction dynamics. Numerous interconnected channels between porous structures are created spontaneously during the sacrificial fabrication process, penetrating throughout the electrode. They remain unblocked even after fast discharge, shown in Figure 4d−e, in the zoom-in cross-section SEM morphology. Therefore, the blocking issue that has traditionally occurred in high loading Li−S cells is successfully overcome.

Second, the ample pore structure exists as storage space throughout the electrode. This storage space can easily sustain the dissolved polysulfide in the porous structure, as shown in Figure 4d. The polysulfide is kept from diffusing into the open electrolyte, minimizing the shuttle effect. Also, the affinity between the polysulfide and the functionalized binder can improve the storage efficiency. The clear color of electrolyte on



DOI: 10.1021/acs.nanolett.6b01434
Nano Lett. 2016, 16, 5365−5372

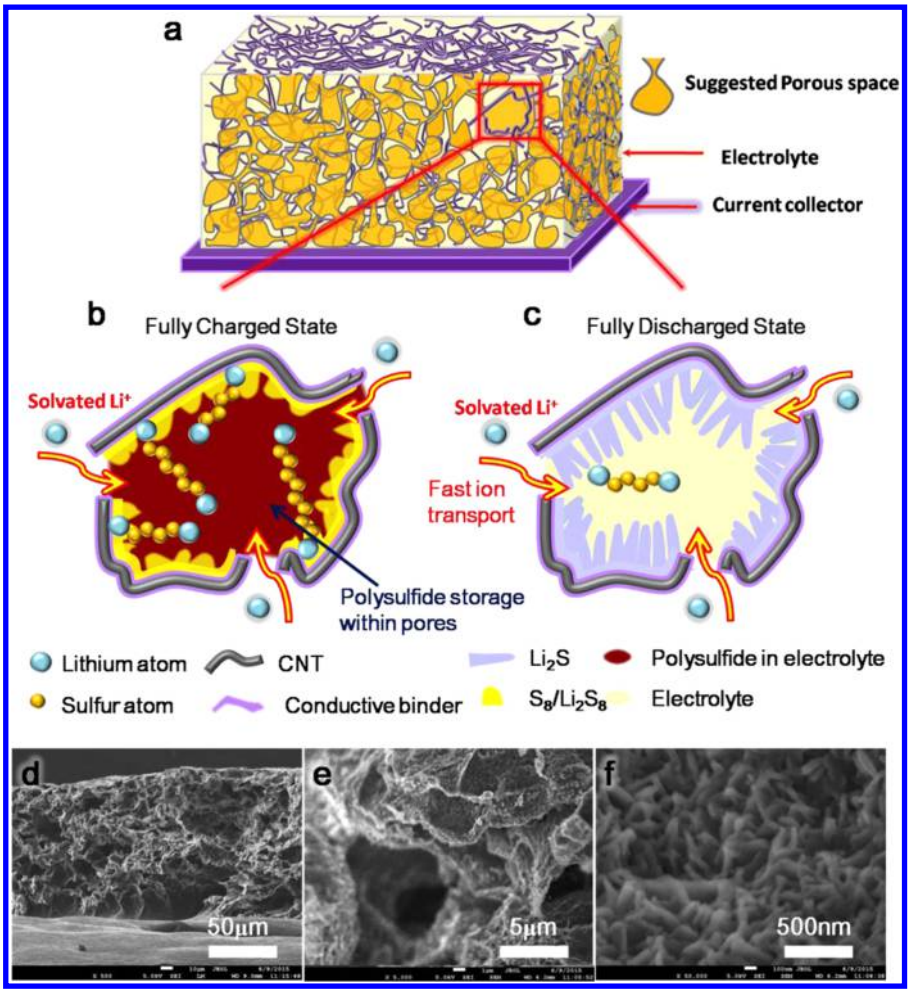


**Figure 4.** Schematic diagram of the CNT-nest-S electrode structure (a) and a local magnification diagrams in fully charged (b) and discharged state (c) to illustrate the working mechanism of the nest structure electrode. (d–f) SEM images of the cross-section morphology of the CNT-nest-S electrode with 3 mg·cm$^{-2}$ sulfur loading, discharged at C/3 after two C/10 cycles.

the separator from the dissembled cell at fully discharged state shows this reduced effect, shown in the inset of Figure 3a, when comparing with the color of the electrolyte in the CNT-S cell shown in Figure 1b. Third, the conductive binder can help to improve electrode conductivity, while the porous structure with the large surface area of CNT helps to extend the reaction surface area. Therefore, an efficient transformation of the sulfur species is observed during the charge ($S_8$/$Li_2S_8$) and discharge process ($Li_2S$/$Li_2S_2$), demonstrated in Figure 4b–c, and is also proved by the clear electrolyte in the inset of Figure 3a. This research demonstrates—via the good performance of high loading Li–S cells—the effectiveness of an efficient Li–S electrode that mimics the beauty of an ant-nest structure.

The difference in the morphology of the sulfur species in the fully charged state ($S_8$/$Li_2S_8$) and discharged state ($Li_2S$/$Li_2S_2$) is depicted in Figure 4b and c. The semitransparent yellow region with the blurred edge refers to the elemental sulfur ($S_8$) or the long chain polysulfide ($Li_2S_8$).[37−39] The needle-shaped structure is drawn in Figure 4c to depict the morphology of $Li_2S$/$Li_2S_2$. An interesting morphology of the needle-shaped structure is observed inside the micropores at fully discharged state in CNT-nest-S electrode, with high magnification SEM in Figure 4f. All of the inner walls inside the pores are covered by this needle-shaped structure, which is smaller than 50 nm in diameter and approximately 200 nm in length. A large relative ratio of sulfur is observed by EDX, and a capacity of more than 900 mA·h·cm$^{-2}$ is obtained. XRD characterization of the sulfur species is performed in this fully discharged state, and the needle-shaped sulfur species may be assigned to be $Li_2S$, shown in Figure S3. It is interesting that the needle structure is very sensitive to electron beam irradiation. Figure S4a–i shows the SEM images taken continuously on the same spot in Figure S4a. The needle-shaped structure will gradually sputter away after continuous expose to electron beam in SEM, and only bare CNT framework, underlying the needle-shaped structure, will be left. Although not thoroughly reported in other research, this needle-shaped structure could possibly be $Li_2S$ nanowires grown on the CNT surface. Analogous to the nanowire growth in other inorganic systems, the needle-shaped structures are guessed to be the result of surface tension, discontinuous crystal structure growth in initial atom layers, and the subsequent precipitation.[40,41] The extended high conductive surface area of the electrode decreases the current density; therefore, it promotes growth of the $Li_2S$ crystal along its preferred crystal direction.[42,43] In comparison, blanket-shaped $Li_2S$ covers the whole surface area of CNT-S; no nanostructure is observed on the surface, as shown in the inset of Figure 1a. The ant-nest structure of the CNT-nest-S electrode has more assessable electrode surface area for sulfur species precipitation. Therefore, the current density is much lower throughout the CNT-



DOI: 10.1021/acs.nanolett.6b01434
Nano Lett. 2016, 16, 5365−5372

nest-S electrode, kinetically favoring the directional $Li_2S$ crystal growth rather than homogeneous blanket precipitation. Furthermore, the needle-shaped $Li_2S$ has less blocking effect to the lithium ion transport in CNT-nest-S, than the blanket coverage in CNT-S. This further shows the positive effect of CNT-nest-S electrodes in assisting polysulfide precipitation with the enlarged, high-conductive surface and unblocked ion transport pathway.

The characteristics of the ant-nest structure are further demonstrated in the detailed comparison between the CNT-nest-S and regular CNT-S. When fast discharge is applied on the high loading CNT-S cells, the sulfur species precipitate on the surface of the electrode and block channels from further reaction, as shown in the Figure 1a inset. A large quantity of bare CNT network is observed in TEM with a very small amount of observable $Li_2S$ precipitation, shown in Figure S5a,b. On the CNT-nest-S, the edges of the entire surface are covered by $Li_2S$ precipitation, with the CNT network being not clearly observable, and small random pores still visible (shown in Figure S5c,d). This difference in sulfur distribution is also observed in EDX mapping. Very little sulfur content and high carbon levels are detected in the regular CNT-S electrode, shown in Figure S6a–c, while more sulfur content is detected all over the scan area in the CNT-nest-S electrode, shown in Figure S6d–f. A larger relative quantity of the sulfur to carbon content is observed in CNT-nest-S with EDX. In CNT-nest-S, the relative S to C ratio is 0.38, which is 19 times higher than in the regular CNT-S electrode.

Another major challenge addressed in this research is the low sulfur ratio of Li–S electrodes applied in the current Li–S system—usually below 60 wt % (to total electrode mass). As discussed frequently in recent researches, the high fraction of nonactive material decreases electrode level capacity and significantly lowers the energy density of a Li–S battery,[24,34,35] which is highly undesirable. Although several attempts have been made toward a higher sulfur ratio electrode, the results have not been satisfactory. The novel nest-structure electrode proposed in this work demonstrates good cycling and rate performance on high-loading Li–S batteries, and its potential can be further achieved in ultrahigh sulfur ratio (up to 85 wt %) application.

The ant-nest structure's ability to allow ultrahigh sulfur ratio Li–S batteries is first demonstrated by the 80 wt % sulfur in composite electrode (named CNT-nest-80%S), which is composed solely of 80 wt % sulfur, 5 wt % binder, and 15 wt % CNT. All cells have sulfur loading levels ranging from 2.5 $mg{\cdot}cm^{-2}$ to 3.0 $mg{\cdot}cm^{-2}$. The cycling performance is plotted in Figure 5a. A high capacity of 1123.5 $mA{\cdot}h{\cdot}g^{-1}$ is achieved at C/10 (167 $mA{\cdot}g^{-1}$) and 908.5 $mA{\cdot}h{\cdot}g^{-1}$ is obtained at C/3 (558 $mA{\cdot}g^{-1}$) for the CNT-nest-80%S cell. Moreover, a high capacity of 937 $mAh{\cdot}g^{-1}$ can be achieved at C/10 (167 $mA{\cdot}g^{-1}$) for the CNT-nest-85%S cell (85 wt % sulfur, 3 wt % binder, and 12 wt % CNT), with stable performance of 800 $mA{\cdot}h{\cdot}g^{-1}$ over 80 cycles, shown in Figure S7. In this way, the battery makes full use of the ant-nest structure and increases the sulfur loading at the same time—with significant decrease in the ratio of the nonactive material.

To better understand the ant-nest structure mechanism with a high sulfur loading and a high sulfur ratio, post-mortem analysis of the cycled cell is performed with CNT-nest-80%S after two cycles at C/10 followed by one discharge at C/3. Cross-section morphology of the CNT-nest-80%S cell is observed through SEM in Figure 5b,c. As shown, the ant-nest

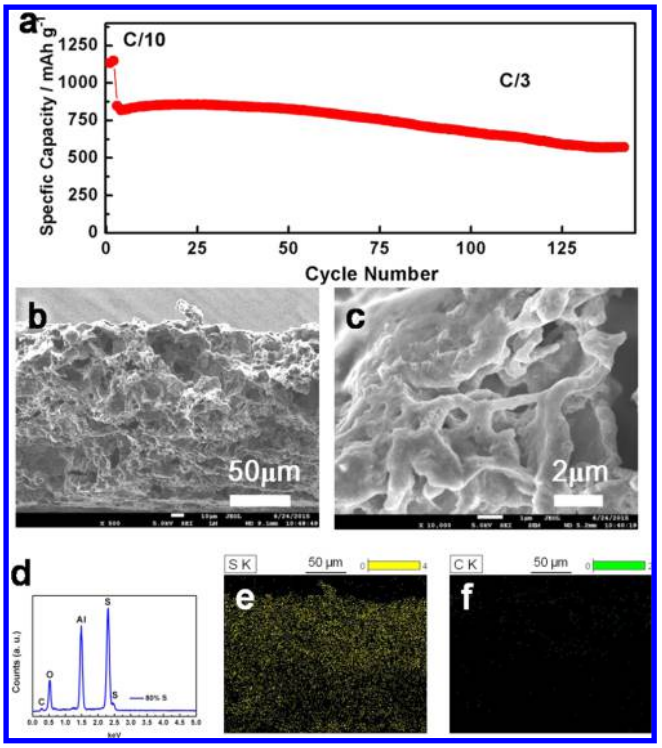


**Figure 5.** (a) Cycling performance of the CNT-nest-80%S cell. SEM images of cycled CNT-nest-80%S electrodes cross-section morphology (b) and zoom-in morphology (c). EDX data (d) and EDX mappings (e, f) for the cycled 80% S-nest-S electrode corresponding to the area shown in b.

structure remains, exhibiting large pores and unblocked interconnected channels. A very thick $Li_2S$ precipitation layer is observed coating the surface of the CNT network. This indicates that, with the assistance of a highly conductive CNT network and conductive binder, the reaction surface is highly efficient for resistive $Li_2S$ precipitation. Also, the numerous porous structures can provide enough space for a large quantity of polysulfide storage and large surface for efficient precipitation. Noticeable shrinkage of the interconnected channels is observed, but they mostly remain open after the fast discharge; therefore, fast ion transport can be ensured in high loading Li–S cells. Further evidence of the superior capability in sulfur species ($Li_2S$) precipitation is given via EDX, shown in Figure 5d–f. A high relative sulfur to carbon content (S to C ratio: 1.88) is observed: 94 times the regular CNT-S and 5 times the 50%S-CNT-nest-S. EDX mapping further demonstrates the high sulfur composition ratio and full-coverage in the porous structure. The CNT-nest-80%S is completely covered by sulfur species ($Li_2S$) with the CNT framework buried beneath. Therefore, large quantities of sulfur are observable, but carbon signal can hardly be detected, shown in Figure 5e,f. In this way, the unique properties of the ant-nest structure are clearly demonstrated via the hosting of ultra high sulfur ratio in high-loading Li–S batteries. The design idea of the ant-nest structure has been fulfilled: with large storage area and functionality to attract and sustain polysulfide, the multi interconnected channels to assist fast ion transportation, and the highly conductive CNT and conductive binder to ensure the high conductivity of the entire electrode. Further efforts are needed for overall cell optimization.

The novel, nature-derived ant-nest structure Li–S electrode has demonstrated the possibility of achieving electrode-scale



DOI: 10.1021/acs.nanolett.6b01434
Nano Lett. 2016, 16, 5365–5372

production of high-loading, high-sulfur-ratio Li−S batteries that cost little to manufacture and use easy and manufacturing-friendly methods including slurry ball-milling, doctor-blade based laminate casting, and feasible sacrificial methods for creating a porous surface. The sacrificial method, using table salt as a method for creating the biomimetic ant-nest structure, is unique and effective and bypasses some of the complicated and expensive materials or multistep synthesis methods needed to solve the open issues.[14] By recreating the superb, nature-designed, three-dimensional ant-nest structure using table salt, the Li−S electrode obtains the unique properties of the ant-nest structure. By biomimicking the smart spacial design of a porous ant-nest structure, and applying the inner surface decoration with a functional binder, efficient polysulfide suspension is achieved within the porous storage space and enhanced by the strong affinity between the functional binder and polysulfide. Also, the multi-interconnected channels of the ant-nest structure are created spontaneously in the sacrificial synthesis process, which endows ultra fast ion transport capability to the Li−S electrode. The extended inner surface via the porous ant-nest structure provides an extra-large reaction interface for polysulfide transformation and precipitation. The conductive binder, along with the highly conductive carbon nanotube, helps to enhance the conductivity of the reaction interface and long-distance charge transport.

Porous structures are created in two scales: micro- and nanoscale. The nanoscale refers to the space between single nanotubes, which scatter around the micropores and can enable use of the entire large carbon nanotube surface. This marvelous ant-nest structure has shown strong capability in carrying high sulfur loading and can increase the sulfur ratio as high as 85%, with only 12% CNT and 3% conductive binder, which is the same composition of active material as the commercial cathode. The 85% sulfur electrode can not only sustain the mechanical force during polysulfide dissolution and precipitation but also can provide all the necessities for the reaction of high loading Li−S batteries, as discussed above. Both good cycling/rate performance and high sulfur utilization is achieved in this novel, high-loading sulfur electrode, which suggests that the efficient spacial design of the Li−S electrode is indeed the solution to achieving high loading industrialized Li−S batteries.

Further research is still needed to explore the potential of this ant-nest structure. Since the ant-nest structure Li−S electrode is designed with sacrificial household table salt, further research could optimize the micropore through size and distribution control of the sacrificial table salt. Also, improved use of the ultra large surface of the carbon nanotube (nanopores between each nanotube) can be achieved via further control of the solvent evaporation process during doctor-blade laminate casting. Furthermore, in order to improve the stability of the high-loading Li−S batteries, the optimization of the electrolyte composition, and protection of lithium counter electrode should be further studied, via surface protection[44] or addition of additives,[14,45] etc.

In conclusion, this research shows the viability of an electrode-scale nature-inspired ant-nest structure electrode for the application of Li−S batteries. It processes the unique properties of the ant-nest structure of the large polysulfide storage capability and highly efficient, multi interconnected ion transportation pathway design and extended reaction interface to achieve unique direction crystalline sulfur species precipitation on the surface of the CNT.

## ■ ASSOCIATED CONTENT

### Supporting Information

The Supporting Information is available free of charge on the ACS Publications website at DOI: 10.1021/acs.nanolett.6b01434.

Detailed material, fabrication procedures, cell assembly, and characterization techniques (PDF)

## ■ AUTHOR INFORMATION


### Corresponding Author

*Tel.: +1-510-486-7207; e-mail: gliu@lbl.gov.


### Author Contributions

G.A., Y.D., H.Z., and G.L. conceived the idea, designed experiments, and analyzed the data. G.G.A. and W. M. carried out the synthesis of materials and electrochemical tests. G.A., W.M., and X.S. performed the characterization of materials. Y.F., Y.E., V.B., V.S., and G.L. contributed to the discussion of the results. G.A. and G.L. cowrote the paper. All the authors commented and have given approval to the final version of the manuscript.


### Funding

Funding was provided through the Advanced Battery Materials Research (BMR) program from U.S. Department of Energy (U.S. DOE).


### Notes

The authors declare no competing financial interest.

## ■ ACKNOWLEDGMENTS


G.L. acknowledges the support from the Assistant Secretary for Energy Efficiency, Office of Vehicle Technologies of the U.S. Department of Energy (U.S. DOE) under the Advanced Battery Materials Research (BMR) program, along with the National Center for Electron Microscopy of the Molecular Foundry and the Advanced Light Source at the Lawrence Berkeley National Laboratory, which are supported by the U.S. Department of Energy under Contract # DE-AC02-05 CH11231. G.A. and W.M. acknowledge support by the China Scholarship Council.


## ■ ABBREVIATIONS

Li−S, lithium−sulfur; CNT, carbon nanotube; NaCl, table salt or sodium chloride; AB, acetylene black; CNT-nest-S, regular Li−S electrode; CNT-nest-S, ant-nest structure Li−S electrode; CNT-nest-80%S, 80 wt % sulfur ant-nest structure Li−S electrode; CNT-nest-85%S, 85 wt % sulfur ant-nest structure Li−S electrode

## ■ REFERENCES


(1) Tarascon, J. M.; Armand, M. *Nature* **2001**, *414*, 359−367.
(2) Evarts, E. C. *Nature* **2015**, *526*, S93−S95.
(3) Bruce, P. G.; Freunberger, S. A.; Hardwick, L. J.; Tarascon, J. M. *Nat. Mater.* **2011**, *11*, 19−29.
(4) Manthiram, A.; Fu, Y. z.; Su, Y. S. *Acc. Chem. Res.* **2013**, *46*, 1125−1134.
(5) Evers, S.; Nazar, L. F. *Acc. Chem. Res.* **2013**, *46*, 1135−1143.
(6) Manthiram, A.; Fu, Y. z.; Chung, S. H.; Zu, C. x.; Su, Y. S. *Chem. Rev.* **2014**, *114*, 11751−11787.
(7) Mikhaylik, Y. V.; Akridge, J. R. *J. Electrochem. Soc.* **2004**, *151*, A1969−A1976.
(8) Chen, H. w.; Dong, W. l.; Ge, J.; Wang, C. h.; Wu, X. d.; Lu, W.; Chen, L. w. *Sci. Rep.* **2013**, *3*, 1−6.




DOI: 10.1021/acs.nanolett.6b01434
*Nano Lett.* 2016, 16, 5365−5372

(9) Wei Seh, Z.; Li, W. y.; Cha, J. J.; Zheng, G. y.; Yang, Y.; McDowell, M. T.; Hsu, P. C.; Cui, Y. *Nat. Commun.* **2013**, *4*, 1331.
(10) Yang, Y.; Zheng, G. y.; Cui, Y. *Chem. Soc. Rev.* **2013**, *42*, 3018−3032.
(11) Xiao, L. f.; Cao, Y. l.; Xiao, J.; Schwenzer, B.; Engelhard, M. H.; Saraf, L. V.; Nie, Z.; Exarhos, G. J.; Liu, J. *Adv. Mater.* **2012**, *24*, 1176−1181.
(12) Zhou, G.; Yin, L. C.; Wang, D. W.; Li, L.; Pei, S.; Gentle, I. R.; Li, F.; Cheng, H. M. *ACS Nano* **2013**, *7*, 5367−5375.
(13) Seh, Z. W.; Zhang, Q. f.; Li, W. y.; Zheng, G. y.; Yao, H. b.; Cui, Y. *Chem. Sci.* **2013**, *4*, 3673−3677.
(14) Yao, H. b.; Zheng, G. y.; Hsu, P. C.; Kong, D. s.; Cha, J. J.; Li, W. y.; Seh, Z. W.; McDowell, M. T.; Yan, K.; Liang, Z.; Narasimhan, V. K.; Cui, Y. *Nat. Commun.* **2014**, *5*, 4943.
(15) Song, J. x.; Xu, T.; Gordin, M. L.; Zhu, P. y.; Lv, D. p.; Jiang, Y. B.; Chen, Y. s.; Duan, Y. h.; Wang, D. h. *Adv. Funct. Mater.* **2014**, *24*, 1243−1250.
(16) Pang, Q.; Kundu, D.; Cuisinier, M.; Nazar, L. F. *Nat. Commun.* **2014**, *5*, 4759.
(17) Ai, G.; Dai, Y. l.; Ye, Y. f.; Mao, W. f.; Wang, Z. h.; Zhao, H.; Chen, Y. l.; Zhu, J. f.; Fu, Y. b.; Battaglia, V.; Guo, J. h.; Srinivasan, V.; Liu, G. *Nano Energy* **2015**, *16*, 28−37.
(18) Song, J. x.; Gordin, M. L.; Xu, T.; Chen, S. r.; Yu, Z. x.; Sohn, H.; Lu, J.; Ren, Y.; Duan, Y. h.; Wang, D. h. *Angew. Chem., Int. Ed.* **2015**, *54*, 4325−4329.
(19) Scheers, J.; Fantini, S.; Johansson, P. J. *J. Power Sources* **2014**, *255*, 204−218.
(20) Suo, L. m.; Hu, Y. S.; Li, H.; Armand, M.; Chen, L. q. *Nat. Commun.* **2013**, *4*, 1481.
(21) Gordin, M. L.; Dai, F.; Chen, S. r.; Xu, T.; Song, J. x.; Tang, D. h.; Azimi, N.; Zhang, Z. c.; Wang, D. h. *ACS Appl. Mater. Interfaces* **2014**, *6*, 8006−8010.
(22) Yao, H. b.; Yan, K.; Li, W. y.; Zheng, G. y.; Kong, D. s.; Seh, Z. W.; Narasimhan, V. K.; Liang, Z.; Cui, Y. *Energy Environ. Sci.* **2014**, *7*, 3381−3390.
(23) Zhou, G. m.; Li, L.; Wang, D. W.; Shan, X. y.; Pei, S. f.; Li, F.; Cheng, H. M. *Adv. Mater.* **2015**, *27*, 641−647.
(24) Lv, D. p.; Zheng, J. m.; Li, Q. y.; Xie, X.; Ferrara, S.; Nie, Z.; Mehdi, L. B.; Browning, N. D.; Zhang, J. G.; Graff, G. L.; Liu, J.; Xiao, J. *Adv. Energy Mater.* **2015**, *5*, 1−8.
(25) Li, Z.; Zhang, J. T.; Chen, Y. M.; Li, J.; Lou, X. W. *Nat. Commun.* **2015**, *6*, 8850.
(26) Hu, G. j.; Xu, C.; Sun, Z. h.; Wang, S. g.; Cheng, H. M.; Li, F.; Ren, W. c. *Adv. Mater.* **2016**, *28*, 1603−1609.
(27) Yang, Y.; Zheng, G. y.; Misra, S. h.; Nelson, J.; Toney, M. F.; Cui, Y. J. *J. Am. Chem. Soc.* **2012**, *134*, 15387−15394.
(28) Barchasz, C.; Mesguich, F.; Dijon, J.; Leprêtre, J. C.; Patoux, S.; Alloin, F. J. *J. Power Sources* **2012**, *211*, 19−26.
(29) Wang, Q. q.; Wang, W. k.; Huang, Y. q.; Wang, F.; Zhang, H.; Yu, Z. b.; Wang, A. b.; Yuan, K. g. *J. Electrochem. Soc.* **2011**, *158*, A775−A779.
(30) Cheon, S. E.; Ko, K. S.; Cho, J. H.; Kim, S. W.; Chin, E. Y.; Kim, H. T. *J. Electrochem. Soc.* **2003**, *150*, A800−A805.
(31) Latty, T.; Ramsch, K.; Ito, K.; Nakagaki, T.; Sumpter, D. J. T.; Middendorf, M.; Beekman, M. *J. R. Soc., Interface* **2011**, *8*, 1298−1306.
(32) Zhang, Z. y.; Wang, S.; Ding, L.; Liang, X. l.; Pei, T.; Shen, J.; Xu, H. l.; Chen, Q.; Cui, R. l.; Li, Y. *Nano Lett.* **2008**, *8*, 3696−3701.
(33) Liu, G.; Xun, S.; Vukmirovic, N.; Song, X.; Olalde-Velasco, P.; Zheng, H.; Battaglia, V. S.; Wang, L.; Yang, W. *Adv. Mater.* **2011**, *23*, 4679−4683.
(34) Zhou, G. m.; Li, L.; Ma, C. q.; Wang, S. g.; Shi, Y.; Koratkar, N.; Ren, W. c.; Li, F.; Cheng, H.-M. *Nano Energy* **2015**, *11*, 356−365.
(35) Zhang, S. S.; Tran, D. T. *J. Power Sources* **2012**, *211*, 169−172.
(36) Ai, G.; Dai, Y.; Ye, Y.; Mao, W.; Wang, Z.; Zhao, H.; Chen, Y.; Zhu, J.; Fu, Y.; Battaglia, V.; Guo, J.; Srinivasan, V.; Liu, G. *Nano Energy* **2015**, *16*, 28−37.
(37) Diao, Y.; Xie, K.; Xiong, S. z.; Hong, X. b. *J. Electrochem. Soc.* **2012**, *159*, A421−A425.
(38) Patel, M. U. M.; Demir Cakan, R.; Morcrette, M.; Tarascon, J. M.; Gaberscek, M.; Dominko, R. *ChemSusChem* **2013**, *6*, 1177−1181.
(39) Waluś, S.; Barchasz, C.; Colin, J. F.; Martin, J. F.; Elkaïm, E.; Leprêtre, J. C.; Alloin, F. *Chem. Commun.* **2013**, *49*, 7899−7901.
(40) Feng, X.; Shankar, K.; Varghese, O. K.; Paulose, M.; Latempa, T. J.; Grimes, C. A. *Nano Lett.* **2008**, *8*, 3781−3786.
(41) Ai, G.; Sun, W.; Gao, X.; Zhang, Y.; Peng, L. M. *J. Mater. Chem.* **2011**, *21*, 8749−8755.
(42) Elazari, R.; Salitra, G.; Talyosef, Y.; Grinblat, J.; Scordilis Kelley, C.; Xiao, A.; Affinito, J.; Aurbach, D. *J. Electrochem. Soc.* **2010**, *157*, A1131−A1138.
(43) Kubel, F.; Bertheville, B.; Bill, H. *Z. Kristallogr. - New Cryst. Struct.* **1999**, *214*, 302−302.
(44) Li, W. y.; Yao, H. b.; Yan, K.; Zheng, G. y.; Liang, Z.; Chiang, Y. M.; Cui, Y. *Nat. Commun.* **2015**, *6*, 7436.
(45) Aurbach, D.; Pollak, E.; Elazari, R.; Salitra, G.; Kelley, C. S.; Affinito, J. *J. Electrochem. Soc.* **2009**, *156*, A694−A702.



DOI: 10.1021/acs.nanolett.6b01434
*Nano Lett.* 2016, 16, 5365−5372